# Electron microscopy, spectroscopy, and first-principles calculations of Cs$_2$O

S. Gemming[a], G. Seifert[a], C. Mühle[b], M. Jansen[b], A. Albu-Yaron[c], T. Arad[c], R. Tenne[c],*

[a]*Institut für Physikalische Chemie, Technische Universität, Dresden, 01062 Dresden, Germany*
[b]*Max-Planck-Institut für Festkörperforschung, Heisenbergstrasse 1, 70569 Stuttgart, Germany*
[c]*Department of Materials and Interfaces, The Weizmann Institute of Science, Faculty of Chemistry, PO Box 26, 76100 Rehovot, Israel*

## Abstract

Oxides of cesium play a key role in ameliorating the photoelectron emission of various opto-electronic devices. However, due to their extreme reactivity, their electronic and optical properties have hardly been touched upon. With the objective of better understanding the electronic and optical properties of Cs$_2$O in relationship to its structure, an experimental and theoretical study of this compound was undertaken. First-principles density functional theory calculations were performed. The preferred structural motif for this compound was found to be anti-CdCl$_2$. Here three Cs–O–Cs molecular layers are stacked together through relatively weak van-der-Waals forces. The energy bands were also calculated. The lowest transition at 1.45 eV, was found to be between the $K$ point in the valence band to the $\Gamma$ point in the conduction band. A direct transition at 2 eV was found in the center ($\Gamma$) of the Brillouin zone. X-ray powder diffraction, transmission electron microscopy and selected area electron diffraction were used to analyze the synthesized material. These measurements showed good agreement with the calculated structure of this compound. Absorption measurements at 4.2 K indicated two optical transitions with somewhat higher energy (indirect one at 1.65 and a direct transition at 2.2 eV, respectively). Photoluminescence measurements also showed similar transitions, suggesting that the lower indirect transition is enhanced by three nearby minima at 1.5 eV in the Brillouin zone.
© 2004 Elsevier Inc. All rights reserved.

## 1. Introduction

Oxides of alkali metals and particularly those of cesium play an important role in reducing the work-function and thus enhancing the electrical current of photo-cathodes, and in promoting catalytic reactions and oxidation enhancement of various semiconductor surfaces. These technological aspects make the study of cesium oxides of special importance. However, the oxides of cesium are extremely sensitive to the ambient atmosphere, converting into white cesium carbonate upon exposure. This obstacle makes a comprehensive study of these materials very difficult. In particular, the study of cesium oxides using transmission electron microscopy (TEM) and its auxiliary techniques, like electron-diffraction (ED) and energy dispersive X-ray spectroscopy (EDS), requires a special means to transfer the sample safely, which was not possible thus far.

The synthesis of pure cesium oxides was studied in the early days of the 20th century [1–3]. Later studies revealed the crystal structures of these oxides [4,5]. The complex cesium–oxygen phase diagram consists of an unusually large number of oxides among them Cs$_7$O, Cs$_{11}$O$_3$ [6], the stoichiometric Cs$_2$O, and also Cs$_2$O$_2$, Cs$_2$O$_3$ [5], CsO$_2$ [7–9], and CsO$_3$ [7] where the oxygen can be present in the form of molecular ions such as superoxide O$_2^-$ or peroxide O$_2^{2-}$. Cesium oxide (Cs$_2$O) crystallizes in the 3R anti-CdCl$_2$ structure. The unit cell

consists of three $Cs_2O$ molecular layers with rhombohedral arrangement ($R\bar{3}M$) and unit cell parameters: $a = b = 4.256$ Å; $c = 18.990$ Å. In each molecular sheet the layer of oxygen atoms is sandwiched between two layers of cesium atoms in octahedral arrangement [4a,7]. The present work deals with the structure of $Cs_2O$, which was investigated through both theoretical calculations and experimental means.

The energy gaps ($E_g$) of the various cesium oxides and their electron affinities (EA) are not accurately known. Reasonable estimates from light absorption and photoemission measurements for $Cs_2O$ are: $E_g = 2$ eV and EA $= 0.8$ eV [10]. The measured work function for mixtures of cesium oxides was found to be as low as 1 eV ($\sim$1200 nm) [9]. Many studies were performed in order to improve the properties of cesium oxide films as coatings for photocathode front surfaces. Aging of the photocathodes is often related to degradation of the cesium oxide coating. It was found that the highest photo-emissivity and greatest stability of photocathodes is obtained with a cesium to oxygen ratio very close to 2:1 [10–12]. However, this ratio does not necessarily indicate that merely $Cs_2O$ is present in the film. Therefore, the study of the electronic and optical properties of $Cs_2O$ in relationship with its structure is highly warranted.

In the present study, a combination of optical measurements and first-principles density functional theory (DFT) calculations was used to study the electronic structure of $Cs_2O$ in relationship to its structure. High-resolution transmission electron microscopy (HRTEM) imaging was attempted to reveal the previously hidden aspect of the microstructure on a range of scales extending down to atomic dimensions. Absorption and photoluminescence measurements at room and cryogenic temperatures were carried out. Satisfactory agreement was obtained between the calculated and experimental observations.

## 2. Experimental

### 2.1. Computational details

Self-consistent density-functional band structure calculations were carried out in the local density approximation with the program package ABINIT. A plane-wave basis set and norm-conserving pseudopotentials are employed to represent the valence electron density and the core-valence interaction. The semicore shell of Cs was also treated explicitly, because the Cs 5$s$ and 5$p$ bands are quite close to the Fermi level, thus an interaction with the O levels has to be accounted for. With these pseudopotentials converged densities of states are obtained for a kinetic energy cutoff $E_{\text{cut}}^{\text{PW}}$ of the plane waves which is better than 64 Ha

(1 Ha $= 24.2$ eV) and only minor changes occur beyond $E_{\text{cut}}^{\text{PW}} = 100$ Ha.

For an investigation of the structural properties and stacking fault energies the Hellman-Feynman forces on the atoms and the stress tensor components must also converge with respect to $E_{\text{cut}}^{\text{PW}}$. While the forces are already converged for $E_{\text{cut}}^{\text{PW}} = 64$ Ha, the stress tensor components vanish only for $E_{\text{cut}}^{\text{PW}} = 121$ Ha or better. Thus the electronic properties are analysed with $E_{\text{cut}}^{\text{PW}} = 64$ Ha, whereas $E_{\text{cut}}^{\text{PW}} = 121$ Ha is employed for the structural and elastic properties. The $k$-point sampling was $10 \times 10 \times 3$ for the 3R anti-$CdCl_2$ (layered) structure with three formula units in the periodically repeated unit cell and $10 \times 10 \times 10$ for the simple 1H stacking sequence with one formula unit per unit cell.

### 2.2. Synthesis and measurements

Cesium oxide was prepared from the elements. Cesium metal was produced from CsCl (Fluka, p.a. 99%) and Ca (Sigma-Aldrich, 99%) by a reaction under vacuum at $T = 800$ °C and was distilled twice [13,14]. Then, liquid cesium was reacted with a substoichiometric amount of dry oxygen [15]. The raw product was heated at $T = 180$ °C for 3 days under argon ($p = 1$ atm) and was subsequently ground in a stream of dry argon. This cycle was repeated three times. Finally, the excess cesium was removed by sublimation in vacuum at $T = 200$ °C. The as-obtained air-sensitive product has a clear orange color and consists of a single phase.

Optical-absorption and luminescence measurements were carried out with sealed ampoules having flat front surfaces. A double-grating monochromator (HRD, Jobin-Yvon) with a standard tungsten lamp was used along with the photomultiplier (RG942, Hamamatsu). Both absorption and photoluminescence-PL (excitation by Ar ion laser at 514.5 nm) were measured in the range of 500–900 nm at both cryogenic and room temperatures. A special holder was constructed to allow insertion of the sealed quartz ampoule containing the material into the cryostat. The X-ray powder diffraction data of $Cs_2O$ were collected with a linear position-sensitive detector on a Stoe Stadi-P diffractometer (Stoe & Cie GmbH, Germany, Ge-monochromated $MoK\alpha_1$ radiation (wave length $= 0.7093$ Å), $2\theta$ range 4–40°, step 0.01°, 0.2 mm capillary diameter). The data has been calibrated with respect to an external Si-standard. Le-Bail fit has been done using JANA2000 program (V. Petricek, M. Dusek, Jana2000, with the crystallographic computing system: Institute of Physics, Prague, Czech Republic, 2003) with 17 variables refined (background has been modelled by a Legendre 10-terms polynom). Imaging, electron diffraction (ED) and chemical analysis by X-ray energy dispersive spectroscopy (EDS) were performed with a Philips CM120 (120 kV) TEM,

equipped with an EDS system (EDAX model Phoenix microanalyzer). Fast Fourier transform (FFT) of the high-resolution images was obtained by Digital Micrograph software (Gatan). Sample analysis without atmospheric exposure was essential and techniques for manipulation, transferring and mounting (onto gold grids) the sample from the ampoule to the TEM under inert conditions of anhydrous/anaerobic atmosphere were developed.

## 3. Results and discussion

### 3.1. Theory and calculations

#### 3.1.1. Structure

The most stable optimized structure is depicted in Fig. 1. It has the 3R anti-CdCl$_2$ crystal structure, which is characterized by an AbC BcA CaB stacking sequence of Cs and O layers as indicated in Fig. 1. Thus, in accordance with the experimental crystal structure data, the O atoms are surrounded by six Cs neighbors in octahedral arrangement. The lattice parameters of the hexagonal unit cell were optimized and amount to $a = b = 4.28$ Å and $c = 15.49$ Å. The calculated value of $c$ is lower than the value deduced from the TEM experiment (see Section 3.2), which indicates that the non-bonding interaction across the van-der-Waals gap of the structures is overestimated as a consequence of the local-density approximation. The spacing along the $c$ axis is $d_c$(Cs–O) = 2.48 Å within a Cs–O–Cs triple layer and $d_c$(Cs–Cs) = 2.69 Å between adjacent Cs–O–Cs triple layers. This finding is indicative of a stronger binding interaction within the triple layers in comparison with the interaction between adjacent triple layers. In order to quantify this result, the simpler AbC AbC stacked (1H) structure was also studied and was found to be less stable than the 3R structure by 0.176 eV per formula unit. This value corresponds to a very low stacking fault energy between the 3R and the 1H structures of only 0.16 J/m$^2$. Therefore the interaction between adjacent Cs–O–Cs triple layers can be characterized as rather weak. In contrast, the intra-layer stacking fault, which leads to a trigonally prismatic arrangement of Cs ions around O has a considerably higher energy of 2 J/m$^2$. These stacking fault energies are actually comparable with the values obtained earlier for MoS$_2$ [16].

#### 3.1.2. Electronic structure

The density of electronic states (DOS) is given in Fig. 2 for the 3R structure (top) and for the 1H structure (bottom). Four peaks in the occupied region of 3R correspond to semicore and valence states, namely to the Cs 5s states at −22.6 eV, O 2s at −16.7 eV, Cs 5p at −9.3 eV, and the combined DOS of O 2p and Cs 6s at −2.5 eV. The latter value compares well with UV photoemission data of Cs$_2$O, where a very narrow peak appears at 2.6 eV below the Fermi level during the oxidation of a Cs film [17]. For the 1H structure also four peaks are obtained: Cs 5s at −22.6 eV, O 2s at −15.9 eV, Cs 5p at −9.4 eV, and the combined DOS of O 2p and Cs 6s at −1.7 eV. The subvalence 5s and 5p levels of Cs are insensitive towards the particular inter-layer arrangement, because these states are rather localized at the Cs centers and do not participate in the inter-layer interaction. O 2s, O 2p, and Cs 6s experience shifts to lower binding energies when going from the 3R structure to the less stable 1H stacking.
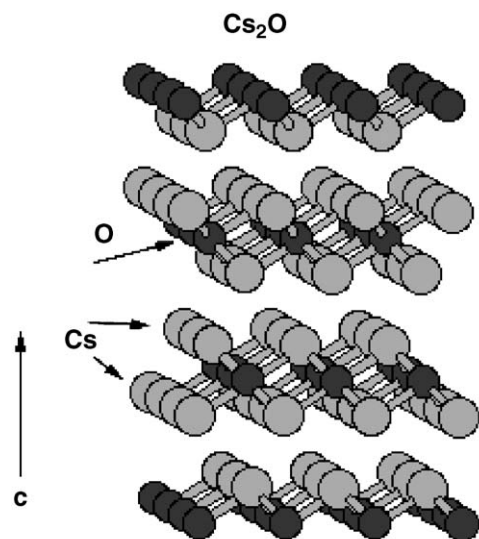


Fig. 1. Schematic illustration of the anti-CdCl$_2$ (3R) structure of Cs$_2$O. Oxygen is in black and cesium in gray.
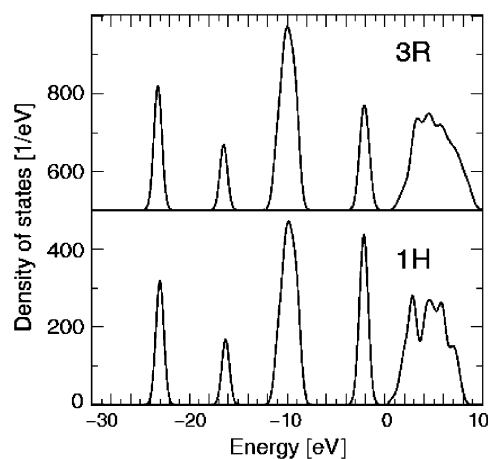


Fig. 2. Calculated density of states of Cs$_2$O. 3R—top; 1H—bottom. The DOS curves are broadened by Gaussian functions of 0.5 eV full width at half maximum.

This result indicates that the weak inter-layer interaction is conveyed mainly by the outermost valence electrons.

For both structures an energy gap separates occupied and unoccupied states; in order to analyse the states spanning this gap in more detail, the band structure of the valence and conduction states were calculated for both the 3R (Fig. 3) and the 1H (Fig. 4) structure. The band structure for the 3R structure is depicted in Fig. 3 within an energy range from −12 to 6 eV. The $k$ points are labelled according to the nomenclature for hexagonal systems. In the 3R structure the Cs $5p$ levels exhibit an overall splitting of 2.7 eV, whereas the valence states are only split by at most 1 eV at the $K$ and $H$ points. This low splitting reflects the weak ligand field of the rather soft Cs cations coordinated to the O anion. In accordance with the symmetry of the 3R stacking sequence the valence levels exhibit no dispersion along the $\Gamma$–$A$ and $M$–$L$ lines. The unoccupied states approach the Fermi level at the $\Gamma$ point with a gap of 2 eV to the uppermost occupied state at $\Gamma$. According to
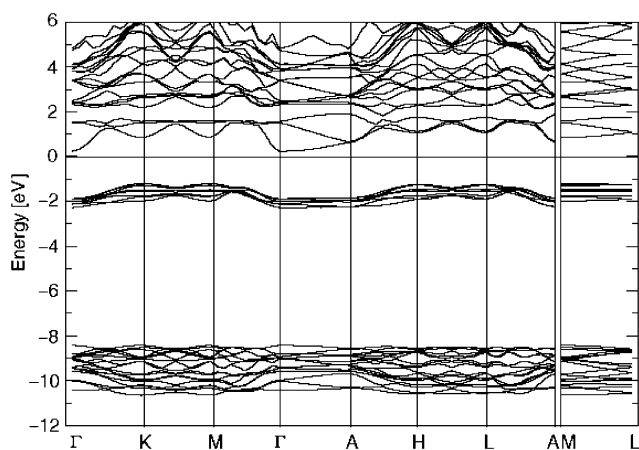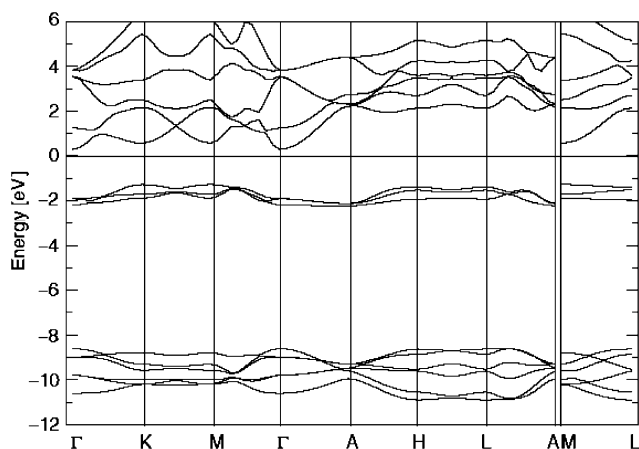
a projection of the corresponding wave function into atomic spheres this lowest unoccupied state is mainly derived from the Cs $6s$ valence levels with only a low admixture of O states. As the valence band maximum occurs at the $K$ points a smaller, indirect energy gap of 1.45 eV results. Slightly larger values of 1.5 eV are obtained for indirect transitions from $M$, $H$, and $L$ to $\Gamma$. Hence, according to the present DFT calculations $Cs_2O$ can be classified as a semiconductor with an indirect gap.

In the 1H structure the semicore $5p$ levels of Cs exhibit a maximum dispersion of about 2.7 eV at $\Gamma$, $H$, and $L$, and a minimum of 0.5 eV at A (Fig. 4). The set of mainly O $2p$ valence bands starts at −2.2 eV ($\Gamma$, $A$). As for the 3R structure the energy gap at the $\Gamma$ point amounts to about 2 eV. For the 1H structure metal-derived bands contribute to unoccupied states close to the Fermi level especially at the $\Gamma$, $K$, and $M$ points. On the average the conduction band edge is located above the valence band by 2 eV for $k_c = 0.0\,1/c$ and by 4 eV for $k_c = 0.5\,1/c$. Thus an indirect gap of 1.5 eV is obtained for the transition from K (and M) to $\Gamma$, which is similar to the electronic properties of the ground state 3R phase. These values should be regarded as a lower bound for the experimentally observed band gaps, because DFT calculations intrinsically tend to underestimate the size of the band gap.

Fig. 5 gives the electron density distribution in a cut plane which is spanned by the [11–20] and [0001] directions. In this plane all three basis atoms are comprised as indicated in the figure. The AbC AbC AbC stacking sequence of the 1H structure (left panel) and the CaB AbC BcA stacking of the 3R structure (right panel) can be clearly distinguished. The valence electron density is strongly delocalized with a peak located at the O sites, and some smaller maxima within the octahedral coordination sphere around the O site and also in the interlayer region. As already concluded on the basis of the DOS plots, the subvalence density remains at the Cs sites, has only minor overlap with the valence density maximum at the O site, and does not participate in a directed interaction across the interlayer region.
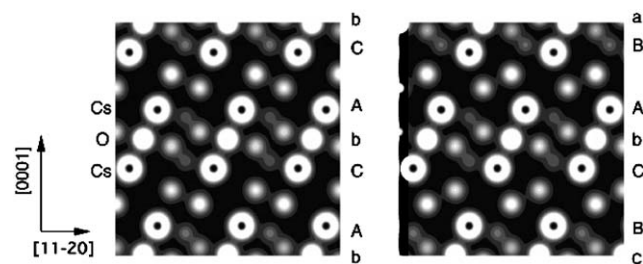


Fig. 3. Band structure for the 3R structure of $Cs_2O$.



Fig. 4. Band structure of 1H structure of $Cs_2O$.



Fig. 5. Electron density distribution in $Cs_2O$ with two different structures. Left—1H; right—3R.

## 3.2. XRD analysis

Fig. 6 shows the experimentally determined X-ray powder diffraction of the powder and the fitted pattern according to 3R-$Cs_2O$ (PDF #09-0104) file. This analysis clearly shows that the probed material is the layered $Cs_2O$ with 3R-anti $CdCl_2$ structure. The calculated cell parameters are: $a = 4.2514(1)$ Å, $c = 18.984(1)$, which agree very well with the published data: $a = 4.256(4)$ Å, $c = 18.990(2)$ Å [4a].

## 3.3. TEM analysis

TEM analysis of the $Cs_2O$ specimens was particularly difficult, because of the bending and/or of the random movement of the crystals (attributed to electron beam induced charging), during examination. Thus, in practice, it was quite difficult to tilt a crystal to the exact zone axis, because of its drift and continuous change of orientation relative to the electron beam. Fig. 7 shows the (HRTEM) image of a $Cs_2O$ crystallite taken from the $Cs_2O$ powder sample (a), the Fourier transform (FFT) (inset b), and the intensity profile from the black framed region in a (inset c). The HRTEM image clearly reveals the intrinsic lamellar structure of the material. The distance between the layers (6.32 Å) matches the Fourier Transform (FFT) results and the line profile results (6.38 Å) for the (0003) points, a typical value for $c/3$ in $Cs_2O$. Fig. 8 is a typical selected-area electron diffraction (SAED) pattern of the $Cs_2O$ sample. The SAED pattern exhibits rings made of the superposition of spotted rings on fairly sharp and continuous rings, indicative of both small particles as well as larger ones. The diffraction pattern can be readily indexed as of the hexagonal $Cs_2O$ structure. These results are in good
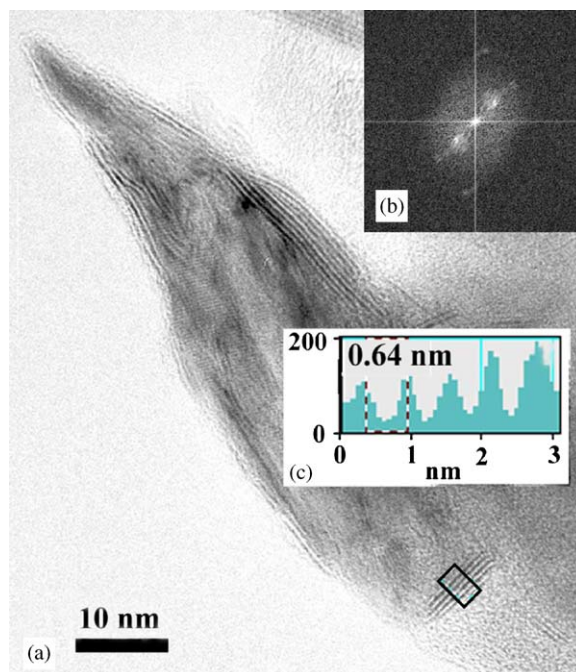


Fig. 7. (a) TEM image showing the typical crystalline microstructure of the $Cs_2O$ sample; note that at locations when orientation is at optimum defocus conditions in the electron beam of the microscope, its intrinsic layered structure is clearly disclosed; (b) FFT and (c) intensity line profile from the black framed marked region in (a).
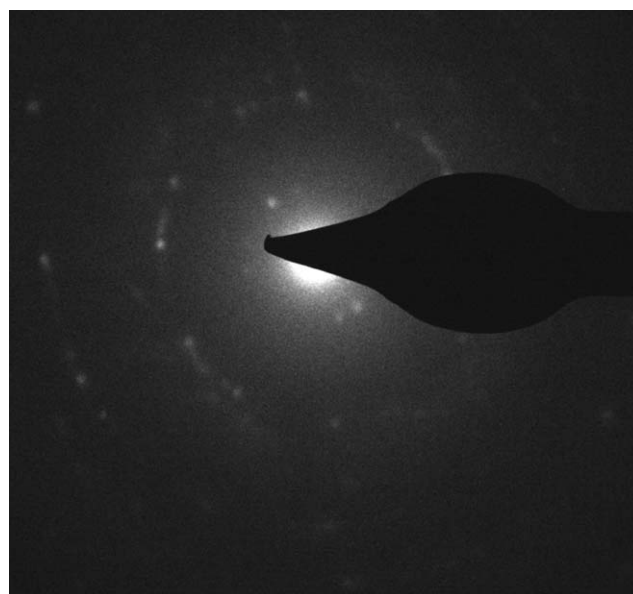


Fig. 8. Selected Area Electron diffraction pattern of the $Cs_2O$ sample.

agreement with those of the X-ray diffraction measurements. Elemental analysis by EDS further confirmed the presence of both Cs and O in the ratio Cs:O~2:1, suggesting the $Cs_2O$ phase.
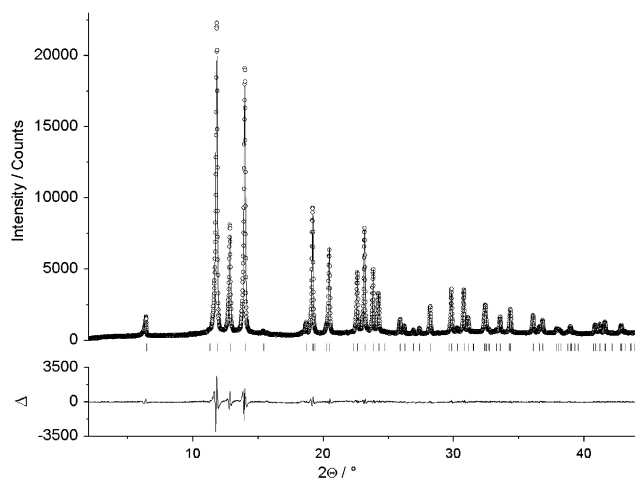


Fig. 6. XRD of the product and fitting with peak indexing according to the file: 3R-$Cs_2O$. Δ represents the deviation of the fitted pattern from the experimentally determined one.

### 3.4. Spectroscopy

Fig. 9 shows a typical optical absorption spectrum of $Cs_2O$ at room temperature. Two absorption gaps are clearly observed a weak absorption edge around 1.65 eV and a stronger absorption edge at 2.1 eV. This spectrum coincides quite favorably with the results of the DFT calculations, which suggest an indirect band gap at 1.45 eV and a direct gap at 2.0 eV. Indeed, a plot of the $(absorption)^2 \times h\nu$ vs. $h\nu$ yields a straight line [18]. Extrapolation of this line to zero absorption yields a band gap of 2.27 eV. Similar measurements with a few other samples yielded values for the band gap in the range of 2.1–2.25 eV. The low absorption edge was fitted using the formula $(absorption)^{1/2} \times h\nu$ vs. $h\nu$, yielding an indirect gap of 1.67 eV. The XRD peaks' width (Fig. 6) clearly shows that the powder consists of particles with micron-size large particles. Therefore, scattering of the light, which is important for the analysis of the optical properties of nanoparticles, is not expected to influence the presently measured absorption spectrum [19].

The PL spectra of $Cs_2O$ at various temperatures are shown in Fig. 10. In accordance with the absorption measurements and the DFT calculations, two distinct transition bands are observed. Whereas at room temperature, a high energy transition is obtained at app. 1.95 eV, a low energy transition is observed at 1.65 eV. Fig. 11 shows the influence of the light excitation intensity on the PL spectrum at 4.2 K. Two wide peaks at 1.65 and 1.95 eV are clearly revealed. As the excitation intensity increases, the low energy transition becomes more pronounced, which is quite unusual for optical transitions in semiconductors. The first-principles calculations indicated that the low energy transition (1.5 eV) is indirect. One would not expect strong PL from this kind of transition. Nonetheless, the $K$–$\Gamma$ lowest energy transition can be enhanced by contributions from the $H$, $M$ and $L$ points in the valence band to the $\Gamma$ point in the conduction band.

An alternative explanation to the appearance of the two peaks would be some spatial non-uniformity, or an impurity level. Since low temperature PL is very sensitive to small ($<0.1\%$) deviations from stoichiometry, like vacancies and interstitials, it is not impossible that the low edge transition at 1.65 eV is associated with deep imperfections of this kind. Local symmetry breaking by vacancies and impurities is known to be a major factor in enhancing the PL of indirect bandgap materials, such as GaP [20], or Cl-doped 2H-$MoS_2$ [21]. The low energy transition is observed clearly also by the absorption measurements (Fig. 8). These measurements are known to be much less sensitive to minute concentrations of impurities or lattice disorder than the PL measurements. This discussion leads to the conclusion that, in accordance with the theoretical results, the low energy transition observed in this work around 1.6 eV emanates from the genuine electronic structure of $Cs_2O$. It is well known that DF theory underestimates the electronic transitions in solids, which may explain the small discrepancy between theory and experimental results. Further explanation for this discrepancy lies in the uncertainty of the optical data of $\pm 0.05$ eV.
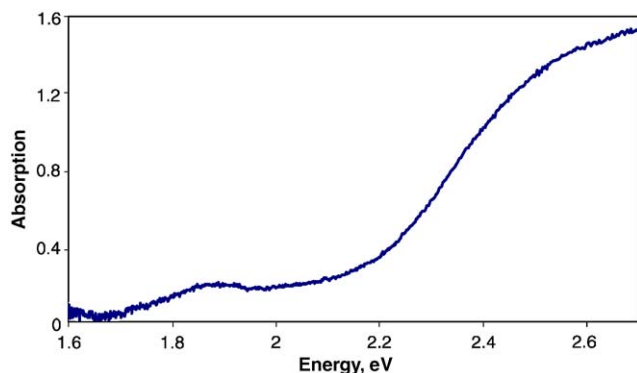


Fig. 9. Absorption spectrum of $Cs_2O$. The indirect (1.67 eV) and the direct gaps (2.27 eV) are clearly observed.



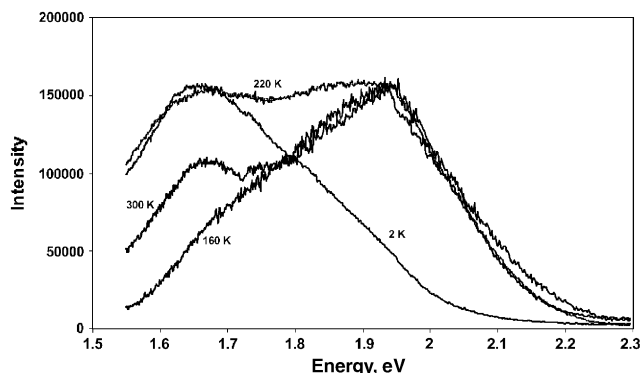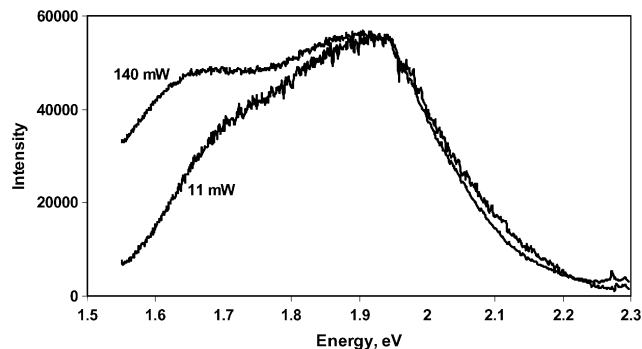Fig. 10. Photoluminescence spectra of $Cs_2O$ at various temperatures.



Fig. 11. Effect of the excitation light intensity on the photoluminescence spectra at 4.2 K.

## 4. Conclusions

The layered compound $Cs_2O$ was synthesized and investigated both theoretically by density-functional band-structure calculations and experimentally by optical absorption, luminescence, and transmission electron microscopy measurements. $Cs_2O$ crystallizes preferably in the anti-$CdCl_2$ structure (3R). The gross structural parameters were obtained in good agreement both by TEM experiments and density-functional calculations. The van-der-Waals gap between adjacent Cs–O–Cs triple layers is underestimated in the calculation as a consequence of the local density approximation. Nevertheless, the inter-layer interaction across the van-der-Waals gap is weak as indicated by the low stacking fault energy calculated for the 1H structure ($0.12\,J/m^2$).

The analysis of the electronic and optical properties shows that $Cs_2O$ is a large-gap semiconductor, which exhibits two intrinsic energy gaps at 1.5–1.7 eV and 1.9–2.2 eV with different temperature dependence in the photoluminescence measurements. Two distinct transitions are also obtained from the density-functional calculations, an indirect $K$ ($H$, $M$, $L$)—$\Gamma$ one at 1.45 eV and a direct one of roughly 2 eV at $\Gamma$. It is thus tempting to assign the two signals in the absorption and luminescence measurements to the indirect and direct electronic transitions found in the calculation of the pristine, defect-free 3R structure. Judging from the temperature and excitation energy dependence of the photoluminescence signals it can, however, not be excluded, that the peak at lower transition energy is enhanced by the presence of an impurity level.

## Acknowledgment

## References

[1] J.L. Howe, J. Am. Chem. Soc. 29 (1907) 384.
[2] R. Marquis, Bull. Soc. Chem. 1 (1907) 169.
[3] (a) E. Rengade, Ann. Chim. Phys. [VIII] 11 (1907) 379;
     (b) E. Rengade, Ann. Chim. Phys. [VIII] 11 (1907) 381.
[4] (a) K.R. Tsai, P.M. Harris, E.N. Lassettre, J. Phys. Chem. 60 (1956) 338;
     (b) K.R. Tsai, P.M. Harris, E.N. Lassettre, J. Phys. Chem. 60 (1956) 347.
[5] A. Helms, W.Z. Klemm, Z. Anorg. Allg. Chem. 242 (1939) 201.
[6] A. Simon, Struct. Bond. 36 (1979) 82.
[7] W. Hesse, W. Schnick, M. Jansen, Prog. Solid State Chem. 19 (1989) 47.
[8] R. Schwartz, G. Brauer, Z. Anorg. Chem. 255 (1947) 102.
[9] N.N. Greenwood, A. Earnshaw, Chemistry of the Elements, Pergamon Press, Oxford, 1984, pp. 97–100.
[10] P.G. Borzyak, V.F. Bibik, G.S. Kramerenko, Bull. Acad. Sci. USSR Phys. Ser. 20 (1956) 939.
[11] C.C. Phillips, A.E. Hughes, W. Sibbett, J. Phys. D: Appl. Phys. 17 (1984) 611.
[12] A.H. Sommer, J. Appl. Phys. 51 (1980) 1254.
[13] L. Hackspill, Helv. Chim. Acta 11 (1928) 1008.
[14] G. Brauer, Handbuch der Präp. Anorg. Chem. Enke-Verlag Stuttgart 2 (1978) 938.
[15] G. Brauer, Handbuch der Präp. Anorg. Chem. Enke-Verlag Stuttgart 2 (1978) 953.
[16] Y. Rosenfeld Hacohen, R. Popovitz-Biro, Y. Prior, S. Gemming, G. Seifert, R. Tenne, Phys. Chem. Chem. Phys. 5 (2003) 1644.
[17] P.E. Gregory, P. Chye, H. Sunami, W.E. Spicer, J. Appl. Phys. 46 (1976) 3525–3529.
[18] J.I. Pankove, Optical Processes in Semiconductors, Dover Publications, Inc., New York, 1971.
[19] A. Usami, Solar Energy Mater. Solar Cells 62 (2000) 239.
[20] L. Merz, R.A. Faulkner, P.J. Dean, Phys. Rev. 188 (1969) 1228.
[21] L. Kulyuk, L. Charron, E. Fortin, Phys. Rev. B 68 (2003) 075314.